Image-based data corrections for Positron Emission Mammography

Nuno C. Ferreira, Fabiana Rodrigues, Luís Martins, Catarina Ortigão, Francisco Caramelo, Luís Mendes, Cláudia S. Ferreira, Pedro Almeida, Miguel Castelo-Branco, and João Varela

***Abstract*–ClearPEM is a rotating, dual planar detector PET system dedicated to breast and axilla imaging that needs data corrections in order to improve quantification and lesion detectability. Since the scanner does not have CT nor transmission sources, we are implementing data corrections that use emission-only data. Also, since in this work we are using an iterative list-mode reconstruction algorithm that projects the data directly through a 3D grid of points, all the corrections are applied in image space. We describe the current implementation and validation of image-based corrections for normalization, scatter, attenuation and randoms. Normalization correction uses sensitivity images generated by backprojecting data from a planar source. Energy-based scatter correction is applied using the Estimation of Trues Method because this method does not require information about attenuating media and takes into account the activity outside the FOV. Attenuation correction is calculated from the segmentation of the breast in the emission images. Randoms correction is performed by subtraction of a smoothed image obtained from the backprojection of the delayed coincidences. The implementation of other corrections is also being pursued in order to obtain fully quantitative images in breast imaging.**

I. Introduction

In Positron Emission Mammography (PEM), data corrections are important not only to allow for semi-quantitative image analysis using SUVs (Standardized Uptake Values) and to obtain a more accurate description of the true activity in the Field Of View (FOV), but also because some data corrections are susceptible of improving detectability, i.e., the ability of the system to discriminate between lesions and healthy tissue.

In this work, we present results of our current effort to develop data corrections for breast imaging, with the goal of achieving quantitative images and improving lesion detectability with the ClearPEM scanner - a rotating, dual planar detector PET system dedicated to breast and axilla imaging.

Since ClearPEM is a PET-only system and neither CT nor transmission sources are available, we have been developing data corrections using emission-only data. Also, since we are using an ML-EM iterative LOR-based list-mode reconstruction that does not require data binning into sinograms or similar histograms, we are applying the developed corrections in the image domain, directly using the coordinates of the measured Lines Of Response (LORs).

II. Methods

A. Normalization correction

Normalization correction is accomplished using sensitivity images that compensate for spatial variations of sensitivity. For each angle that is to be acquired during a breast or axilla study, one sensitivity image is generated by simple backprojection using the projector of the image reconstruction algorithm with the data acquired during a long acquisition of a planar source of activity (Fig. 1). This source is placed parallel to the two detector heads, at middle distance. The planar source data is acquired in a single angular position, but before backprojection the list-mode data is rotated for the same acquisition angles that will be used in the studies where normalization correction is to be applied. Thus for a breast study, where the detector heads are placed in 4 angular positions, 4 sensitivity images are generated (Fig. 1). In axilla imaging, 3 different angles are used, with a different distance between detector heads. Figure 2 shows examples of breast studies with normalization correction.

The normalization method can be applied for a specific energy window, allowing for the easy application of energy-based scatter corrections such as the one described below.

B. Scatter correction

We implemented an image-based version of the Estimation of Trues Method (ETM) [1] for scatter correction. Since transmission data is not available in ClearPEM, single scatter simulation methods [2] such as the ones used in conventional scanners with CT or transmission sources cannot be used (unless transmission is estimated in some way). The large amount of activity outside the Field Of View would also potentially compromise the performance of these algorithms. For these reasons, we use an energy-based method that is easy

Nuno C. Ferreira, Luís Mendes and Miguel Castelo-Branco are with the ICNAS – Instituto de Ciências Nucleares Aplicadas à Saúde, Universidade de Coimbra, Portugal and the IBILI/FMUC - Inst. Biomédico de Investigação da Luz e Imagem, Universidade de Coimbra, Portugal.

Fabiana Rodrigues and Luís Martins are with the ICNAS – Instituto de Ciências Nucleares Aplicadas à Saúde, Universidade de Coimbra, Portugal.

Francisco Caramelo is with the IBILI/FMUC - Instituto Biomédico de Investigação da Luz e Imagem, Universidade de Coimbra, Coimbra, Portugal.

Catarina Ortigão and João Varela are with the LIP - Laboratório de Instrumentação e Física Experimental de Partículas, Lisboa, Portugal.

Cláudia S. Ferreira is with the LIP - Laboratório de Instrumentação e Física Experimental de Partículas, Lisboa, Portugal and the IBEB/FCUL - Instituto de Biofísica e Engª Biomédica, Lisboa, Portugal.

Pedro Almeida is with the IBEB/FCUL - Instituto de Biofísica e Engª Biomédica, Lisboa, Portugal.

to implement in the image domain. Energy-based methods use information from different energy windows, which contain only events with energies between a given LLD (Lower Level Discriminator) and ULD (Upper Level Discriminator).

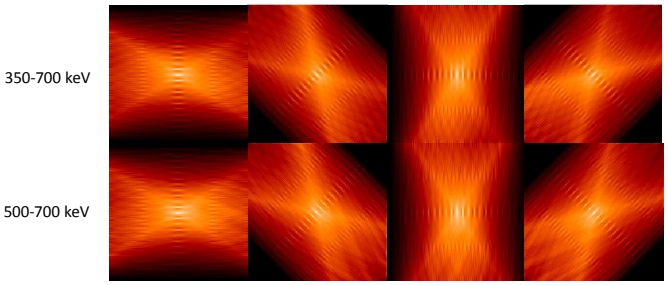

Fig. 1. Sum of all the transaxial slices of the sensitivity volumes generated for each of the acquisition angles used in breast imaging (from left to right: 90º, 135º, 180º and 225º). These sensitivity images can be created for any energy window, allowing the application of an accurate normalization correction to any desired energy window and the easy implementation of energy-based scatter correction methods. Differences related with variations of intrinsic crystal efficiency are visible between the top (350-700 keV) and bottom (500-700 keV) rows, illustrating the need to use energy-adjusted normalization correction.

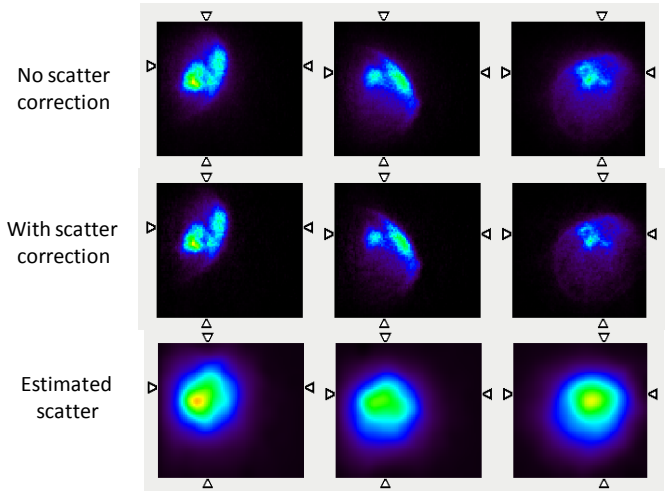

Fig. 2. Individual 2mm slices along the three axes of the reconstructed volume for a patient breast. The top and middle rows show the images without and with the ETM scatter correction, respectively. The bottom row shows the estimated scatter distribution in the reconstructed volume. In each row, the color scale is normalized to the maximum of each volume. Randoms and attenuation correction were not applied. Further improvements in contrast and homogeneity of the images are expected if all corrections are applied.

In the ETM method (Fig. 3), the upper energy window is assumed to provide a noisy estimate of the true activity distribution without scatter (in reality, this window still contains some scatter, but if the LLD is set at a sufficiently high value, this component can be very small). This estimate of trues is scaled to the standard energy window, i.e., the window where scatter correction is going to be applied, and subtracted from the standard window data, leaving only a noisy estimate of the scatter distribution (in the standard window). This noisy estimate is then smoothed, resulting in the final scatter estimate for the standard window.

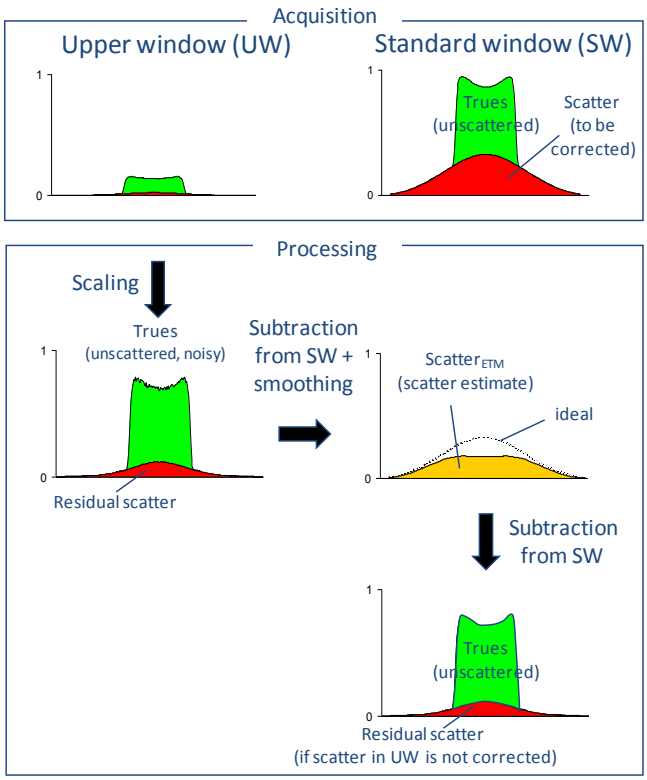

Fig. 3. The Estimation of Trues Method (ETM), an energy-based scatter correction method.

C. *Attenuation correction*

The attenuation correction takes advantage of the approximately constant linear attenuation coefficient (μ) of breast tissue. Hence we assume a constant linear coefficient of attenuation in the breast reducing the problem to the determination of a length that is related to the breast boundaries. The first step of the method consists in the detection of the breast contour by analysis of the gradient of the emission image. The reconstructed images present some background noise and also regions with low contrast, which hamper the segmentation process. Therefore, a contour smoothing routine is applied to remove irregularities in the segmented area, by approximating the detected area to an ellipsoid.

Segmentation permits to calculate the start and end points of the LORs in the breast and to easily determine the length of the LOR in the tissue and in the air (L_{tissue} and L_{air} respectively). The attenuation correction factor for this LOR, which multiplies the value of the event to be backprojected during image reconstruction, is then given by the inverse of the attenuation factor, $e^{-\mu_{tissue}L_{tissue}}e^{-\mu_{air}L_{air}}$.

D. *Randoms correction*

Randoms correction is performed during the list-mode iterative image reconstruction. The prompts data is backprojected at each iteration (one event at a time, using the true LOR information), and at the end of the iteration the volume that results from the backprojection of the delayed

coincidences is smoothed using a Gaussian filter and subtracted from the current prompts reconstructed volume to improve the activity image estimate for the next iteration. The smoothing is applied to reduce noise in the final reconstructed image. The backprojection of a random event may use the same sensitivity image as the one used for prompt events or, if necessary, a sensitivity image calculated only with random events (which may have a different energy distribution than the prompt coincidence events). Another method was recently implemented for the same scanner [3].

E. Decay correction and other corrections

Decay correction is performed for each event before backprojection in image reconstruction. A file with the decay correction value (equal to the inverse of the decay factor, $e^{-\lambda t}$, where t is the time of the event relative to the start of acquisition and λ is the decay constant of the radionuclide) is saved previously to image reconstruction and used in the backprojection of an event.

Corrections for dead time and patient movement are also currently being implemented to attempt to improve the quantification of the images.

F. Validation

The data correction methods described above are being validated using phantom measurements and patient data. Further processing of the data is necessary to evaluate the performance of the methods with different parameters (energy windows, event count-rates, energy window scale factors), acquisition geometries (distance between detector heads), activity distributions and concentrations.

A phantom (Fig. 4) consisting of a 5 cm in diameter cylinder, filled with water (no activity) and placed off-center inside a 10.5 cm in diameter cylinder containing a radioactive solution (water + ^{18}F-FDG, 6 mCi initially) was imaged in the ClearPEM scanner. The inner water cylinder permits to directly visualize uncorrected random and scattered events. Several acquisitions (4 angular positions, 5 minutes in each angle) were made during the decay of the activity in the larger cylinder.

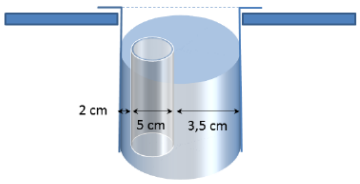

Fig. 4. Phantom used in the validation of the methods.

The data acquired in a study are saved in list mode format, permitting to use *a posteriori* only the desired data for a given energy window. For the initial implementation of the ETM method, we used a standard energy window between 350 and 700 keV and different upper energy windows with LLD ranging from 450 to 550 keV with an ULD of 700 keV. The data from each energy window were corrected for normalization using the method described above, which was applied separately to each of the two energy windows (i.e., planar source data was backprojected using only the events between a given LLD and ULD, resulting in sensitivity images shown in Fig. 1). The ratio of true counts between the upper and the standard windows, measured for the planar source, depends on the specific upper energy window used, but was usually around 10.

To correct for scatter in the phantom results shown in Fig. 6 and Fig. 7, an LLD of 450 keV was used for the upper window. The scale factor between the two energy windows was adjusted visually using the knowledge that the inner cylinder does not contain scatter.

III. Results

The available results are still preliminary. Fully quantitative results are not yet available, since the pipeline of all the data corrections is being implemented and validated. Figs. 2 and 5 show examples of the application of the ETM scatter correction to patient data, where a slight improvement of the contrast can be observed.

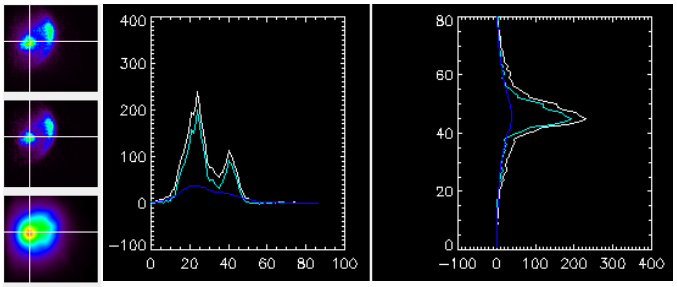

Fig. 5. Left column: images of a breast patient (top: without scatter correction; middle: with scatter correction; bottom: estimated scatter distribution). The horizontal and vertical lines in the images in the first column represent the profiles used to generate the plots seen in the middle and right images respectively (white: without scatter correction; cyan: with scatter correction; blue: estimated scatter distribution).

Figs. 6 and 7 show results of the application of the scatter and random corrections to the phantom in Fig. 4.

IV. Discussion and Conclusion

The upper energy window to be chosen in the ETM scatter correction depends on the specific conditions of the acquisition, such as the number of true events detected and the distance between detector heads.

Some data corrections are still being optimized and validated and many results obtained with phantom experiments are being analyzed. Only after all the data corrections and image reconstruction is finalized and validated we can present final quantitative results.

The ETM scatter correction improves image contrast but only reduces a part of the total scatter if the ratio of the true events in the two energy windows is used. It is possible to

increase the amount of scatter that is subtracted by lowering this scaling factor, but in this case the shape of the estimated scatter distribution may not be the ideal and regions of over/under scatter correction may occur. The phantom results in Fig. 6 and Fig. 7 suggest that this effect may be relatively small. However, the choice of a smaller scaling factor increases the estimated scatter fraction and may lead to an increase of this factor if the random estimate was not correct. This possibility is currently being investigated.

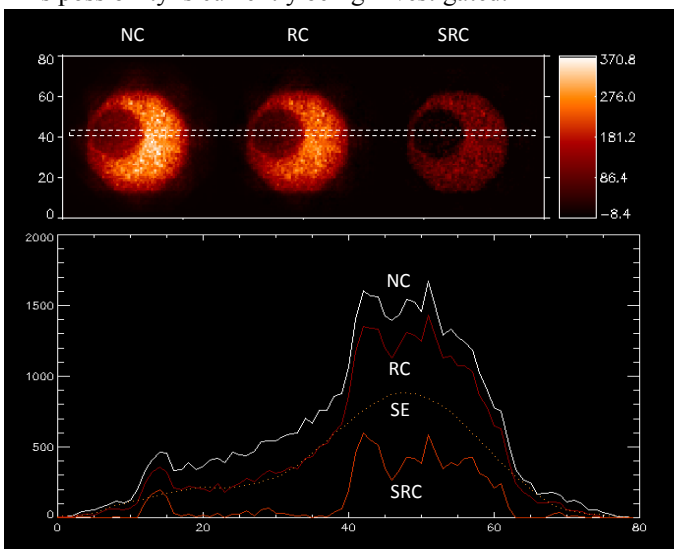

Fig. 6. Application of the random and scatter corrections to the phantom shown in Fig. 3. Attenuation correction was not applied. Upper image: transaxial slice 43 (2 mm thick). From left to right: no randoms and scatter corrections applied ("NC"); randoms correction applied ("RC"); scatter and random corrections applied ("SRC"). The dashed line shows the region used to calculate the horizontal profiles plotted in the bottom. The dotted curve in the plot shows the scatter estimate ("SE").

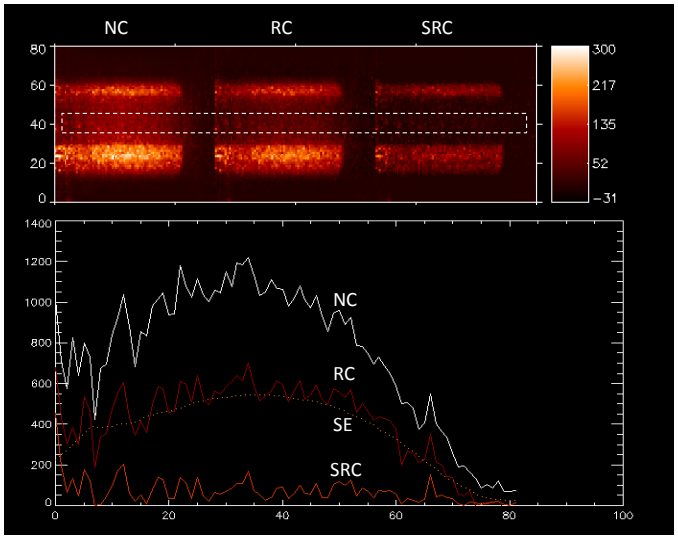

Fig. 7. Application of the random and scatter corrections to the phantom shown in Fig. 3. Attenuation correction was not applied. Upper image: axial slice 25 (2 mm thick). From left to right: no randoms and scatter corrections applied ("NC"); randoms correction applied ("RC"); scatter and random corrections applied ("SRC"). The dashed line shows the region used to calculate the horizontal profiles plotted in the bottom, a region in the inner cylinder that contain only scatter and random events. The dotted curve in the plot shows the scatter estimate ("SE").

Quantification of the breast images in the image domain and without using transmission information seems feasible. In the axillary region a uniform attenuation coefficient cannot be used and a different approach has to be followed for attenuation correction.

ACKNOWLEDGMENT

This work was supported by grant PTDC/SAU-BEB/104630/2008 of FCT (Fundação para a Ciência e a Tecnologia).

REFERENCES

[1] B. Bendriem, R. Trébossen, V. Frouin and A. Syrota, "A PET scatter correction using simultaneous acquisitions with low and high lower energy thresholds", Proceedings of the IEEE NuclearScience Symposium and Medical Imaging Conference, vol. 2, pp. 1237-1242, Toronto, Canada, 1998

[2] C. C. Watson, D. Newport and M. Casey, "A single scatter simulation technique for scatter correction in 3D PET", in Three-Dimensional Image Reconstruction in Radiology and Nuclear Medicine, Eds. P. Grangeat and J.-L. Amans, Doordrecht: Kluwer Academic, Vol. 4, pp. 255-268, 1996

[3] L. Cao, R. Bugalho, C. Ortigão, J. Varela, and J. Peter, "Random Correction Method for Positron Emission Mammography Using Delayed Coincidence Data", Conference Record of the IEEE Nuclear Science Symposium and Medical Imaging Conference, Anaheim, CA, USA, 2012